Supplemental material to this article can be found at:
http://molpharm.aspetjournals.org/content/suppl/2023/01/20/molpharm.122.000546.DC1
1521-0111/103/4/199–210$35.00
MOLECULAR PHARMACOLOGY
dx.doi.org/10.1124/molpharm.122.000546
Mol Pharmacol 103:199–210, April 2023

CRISPR/Cas9-Mediated Induction of Relapse-Specific *NT5C2* and *PRPS1* Mutations Confers Thiopurine Resistance as a Relapsed Lymphoid Leukemia Model[S]

Thao Thu Thi Nguyen, Yoichi Tanaka, Masashi Sanada, Masumi Hosaka, Minori Tamai, Keiko Kagami, Chiaki Komatsu, Shinpei Somazu, Daisuke Harama, Shin Kasai, Atsushi Watanabe, Koushi Akahane, Kumiko Goi, and Takeshi Inukai

Department of Pediatrics, University of Yamanashi, Yamanashi, Japan (T.T.T.N., M.T., K.K., C.K., S.S., D.H., S.K., A.W., K.A., K.G., T.I.); Division of Medicinal Safety Science, National Institutes of Health Sciences, Kanagawa, Japan (Y.T.); and Advanced Diagnostic Research Department, Clinical Research Center, National Hospital Organization, Nagoya Medical Center, Japan (M.S., M.H.)

Received April 20, 2022; accepted January 4, 2023

ABSTRACT

6-Mercaptopurine (6-MP) is a key component in maintenance therapy for childhood acute lymphoblastic leukemia (ALL). Recent next-generation sequencing analysis of childhood ALL clarified the emergence of the relapse-specific mutations of the *NT5C2* and *PRPS1* genes, which are involved in thiopurine metabolism. In this scenario, minor clones of leukemia cells could acquire the 6-MP–resistant phenotype as a result of the *NT5C2* or *PRPS1* mutation during chemotherapy (including 6-MP treatment) and confer disease relapse after selective expansion. Thus, to establish new therapeutic modalities overcoming 6-MP resistance in relapsed ALL, human leukemia models with *NT5C2* and *PRPS1* mutations in the intrinsic genes are urgently required. Here, mimicking the initiation process of the above clinical course, we sought to induce two relapse-specific hotspot mutations (R39Q mutation of the *NT5C2* gene and S103N mutation of the *PRPS1* gene) into a human lymphoid leukemia cell line by homologous recombination (HR) using the CRISPR/Cas9 system. After 6-MP selection of the cells transfected with Cas9 combined with single-guide RNA and donor DNA templates specific for either of those two mutations, we obtained the sublines with the intended *NT5C2*-R39Q and *PRPS1*-S103N mutation as a result of HR. Moreover, diverse in-frame small insertion/deletions were also confirmed in the 6-MP–resistant sublines at the target sites of the *NT5C2* and *PRPS1* genes as a result of nonhomologous end joining. These sublines are useful for molecular pharmacological evaluation of the *NT5C2* and *PRPS1* gene mutations in the 6-MP sensitivity and development of therapy overcoming the thiopurine resistance of leukemia cells.

SIGNIFICANCE STATEMENT

Mimicking the initiation process of relapse-specific mutations of the *NT5C2* and *PRPS1* genes in childhood acute lymphoblastic leukemia treated with 6-mercaptopurine (6-MP), this study sought to introduce *NT5C2*-R39Q and *PRPS1*-S103N mutations into a human lymphoid leukemia cell line by homologous recombination using the CRISPR/Cas9 system. In the resultant 6-MP–resistant sublines, the intended mutations and diverse in-frame small insertions/deletions were confirmed, indicating that the obtained sublines are useful for molecular pharmacological evaluation of the *NT5C2* and *PRPS1* gene mutations.

Introduction

Acute lymphoblastic leukemia (ALL) is the most common childhood malignancy (Inaba and Mullighan, 2020; Malard and Mohty, 2020). Although the prognosis of childhood ALL has dramatically improved (Hunger and Mullighan, 2015; Inaba and Mullighan, 2020; Malard and Mohty, 2020), the prognosis of relapsed ALL remains poor because of drug resistance due to acquired gene mutations of leukemia cells (Ko et al., 2010). In the recent chemotherapeutic regimen for childhood ALL, maintenance therapy is crucial for prolonged remission and relapse prevention (Cortes and Kantarjian, 1995; Wu and Li, 2018; Malard and Mohty, 2020). In maintenance therapy, 6-mercaptopurine (6-MP) in combination with methotrexate is the backbone agent (Wu and Li, 2018; Dieck and Ferrando, 2019; Li et al., 2020). 6-MP is one of the thiopurine analogs that includes 6-thioguanine (6-TG). Recent pharmacogenomic

This work was supported by Japan Society for the Promotion of Science (JSPS) Grants-in-Aid for Scientific Research (KAKENHI) [Grant JP19H03615] and Japan Agency for Medical Research and Development (AMED) [Grant JP19ck0106253].
No author has an actual or perceived conflict of interest with the content of this article.
dx.doi.org/10.1124/molpharm.122.000546.
[S] This article has supplemental material available at molpharm.aspetjournals.org.

ABBREVIATIONS: ALL, acute lymphoblastic leukemia; ddPCR, droplet digital PCR; 5-FU, 5-fluorouracil; HR, homologous recombination; IDT, Integrated DNA Technologies; MBL, Medical & Biologic Laboratories; 6-MP, 6-mercaptopurine; MPA, mycophenolic acid; NHEJ, nonhomologous end joining; *NT5C2*, 5′ nucleotidase II; PAM, protospacer adjacent motif; PCR, polymerase chain reaction; *PRPS1*, phosphoribosylpyrophosphate synthetase 1; RT-PCR, reverse-transcription PCR; sgRNA, single-guide RNA; ssODN, single-strand oligodeoxynucleotide; 6-TG, 6-thioguanine; TIMP, thioinosine monophosphate; ZIP, zero-interaction potency.

analyses reported the association of diverse genetic variants involved in thiopurine metabolism with clinical responses to thiopurine. Namely, loss of hypoxanthine phosphoribosyltransferase 1 (*HPRT1*) activity (Yang et al., 2018), MutS homolog 6 (*MSH6*) haploinsufficiency (Evensen et al., 2018), *NUDT15* polymorphism (Moriyama et al., 2016; Tatsumi et al., 2020), thiopurine *S*-methyltransferase (*TPMT*) and inosine triphosphate pyrophosphatase (*ITPA*) variants (Wahlund et al., 2020) are also reportedly involved in thiopurine metabolism.

In addition to these genetic variants, recent next-generation sequencing analyses revealed a close association of relapsed ALL with acquired point mutations of the essential genes involved in the thiopurine metabolism, including the cytosolic 5′ nucleotidase II (*NT5C2*) and the phosphoribosylpyrophosphate synthetase 1 (*PRPS1*) genes (Meyer et al., 2013; Li et al., 2015, 2020; Dieck et al., 2018; Somazu et al., 2021). NT5C2 plays a crucial role in the de novo purine synthesis pathway, which hydrolyzes inosine 5′-monophosphate (IMP) and other purine nucleotides (Meyer et al., 2013; Tzoneva et al., 2013; Dieck et al., 2018; Tzoneva et al., 2018; Dieck and Ferrando, 2019; Hoell et al., 2019; Li et al., 2020). R238W/L/G/Q, R367Q, D407A/Y/E/H, and R39Q are the most common mutations of the *NT5C2* gene (Dieck et al., 2018; Dieck and Ferrando, 2019). R39Q, R238W/L/G/Q, and R367Q mutations are supposed to disrupt positively charged residues located in the intermonomeric pocket, whereas D407A/Y/E/H mutation is supposed to disrupt the function of the arm region (Dieck and Ferrando, 2019). Therefore, these hotspot mutations disrupt the self-inactivation of NT5C2 and lead to the constitutive activation (Dieck and Ferrando, 2019). On the other hand, PRPS1 catalyzes phosphoribosylpyrophosphate synthesis, which is required for purine synthesis (Li et al., 2015). A190T/V and S103N are the most common mutations of the *PRPS1* gene, which may affect the negative feedback regulation of PRPS1 activity through ADP and GDP, respectively (Li et al., 2015). Of clinical importance, these mutations were generally undetectable in the diagnostic phase (Li et al., 2020). Once minor clones of leukemia cells acquire the relapse-specific mutations of the *NT5C2* or *PRPS1* gene, such clones could be selectively expanded during chemotherapy, including 6-MP treatment as a result of the 6-MP–resistant phenotype (Fig. 1A). Consistently, in our recent analysis of 106 ALL cell lines (Somazu et al., 2021), *NT5C2* and *PRPS1* mutations were exclusively detected in the cell lines established from the samples at relapse and associated with reduced levels of DNA-incorporated thioguanine and, subsequently, inferior thiopurine sensitivities.

To develop a novel therapeutic modality overcoming thiopurine resistance in relapsed ALL cases, human leukemia models that genetically mimic relapse-specific *NT5C2* and *PRPS1* mutations are urgently required. In general, the pharmacological significance of the gene mutation is evaluated in leukemic cell lines transduced with wild-type or mutated cDNA using retroviral vectors. In the case of *NT5C2* and *PRPS1* mutations, thiopurine-resistant phenotypes were confirmed in ALL cell lines transduced with mutated *NT5C2* or *PRPS1* cDNAs using lentiviral vectors (Tzoneva et al., 2013; Li et al., 2015).

Despite its utility, lentiviral vector–mediated gene transfer has several underlying limitations. Lentiviral vector induces overexpression of the target gene derived from cDNA under the control of the viral promoter in addition to background expression of the intrinsic gene. Moreover, cDNA lacks introns and a 3′-untranslated region of the target gene, which are involved in transcriptional and post-transcriptional regulation of gene expression (Sandberg et al., 2008; Mayr and Bartel, 2009; Shaul, 2017). Furthermore, in the *NT5C2* gene, many alternative splicing transcripts were identified by the RNA-sequencing analysis (Black et al., 2018). Similarly, several splicing variants of the *PRPS1* gene were registered in the National Center for Biotechnology Information database. Considering these limitations, direct induction of the hotspot mutations into the intrinsic gene of leukemia cells is the ideal model for pharmacological verification of *NT5C2* and *PRPS1* mutations.

Based on the above scenario in the clinical course of relapsed ALL with the emergence of *NT5C2* or *PRPS1* mutations, we sought to introduce hotspot mutations of the *NT5C2* and *PRPS1* gene into a human lymphoid leukemia cell line via homologous recombination (HR) using the CRISPR/Cas9 system (Fig. 1A). Considering the off-target effect of the CRISPR/Cas9 system, we selected the *NT5C2*-R39Q and *PRPS1*-S103N mutations with the highest off-target scores among hotspot mutations as candidates. In the clinical setting, the *NT5C2*-R39Q mutation was collectively reported in five cases (3.9%) out of 129 relapsed ALL cases with *NT5C2* gene mutations (Meyer et al., 2013; Tzoneva et al., 2013; Dieck et al., 2018; Tzoneva et al., 2018; Dieck and Ferrando, 2019; Hoell et al., 2019; Li et al., 2020), whereas the *PRPS1*-S103N mutation was reported in two cases (11%) out of 18 relapsed ALL cases with *PRPS1* gene mutations (Li et al., 2015, 2020). After the culture in the presence of 6-MP at therapeutic concentration, we successfully obtained the thiopurine-resistant sublines that acquired the intended *NT5C2*-R39Q or *PRPS1*-S103N mutations. Moreover, we also obtained the sublines with diverse in-frame mutations via nonhomologous end joining (NHEJ)-mediated repair, which also conferred thiopurine resistance.

Materials and Methods

Cell Line. KOPN55bi was established from the patient with chronic myeloid leukemia lymphoid blast crisis (Uno et al., 2003), in which clinical characteristics can resemble those of Philadelphia chromosome–positive (Ph^+) ALL (Kolenova et al., 2016; Patel et al., 2021) and was maintained in RPMI 1640 medium supplemented with 10% fetal calf serum.

Introduction of the NT5C2 and PRPS1 Mutations by the CRISPR/Cas9 System. For *NT5C2*-R39Q mutation, the sequences of single-guide RNA (sgRNA) and single-strand oligodeoxynucleotide (ssODN) were 5′- tgtgaaccgaagtttagcaa -3′ and 5′-gctactcaccagcaagggtataatccatatcaaaaccaaaacactttatcttttccatAgcCaaacttTggttcacaaacaccctatagaaaataataaa -3′, respectively. For *PRPS1*-S103N mutation, the sequences of sgRNA and ssODN were 5′-tcctcccctccatttagagc -3′ and 5′-tgtaggtccatggtgataatatgatctgcacctgctacagatagcatatttgcaacaagcttggctgagattggcgcGcggTtctaaatggaggggaggaaagaaaagaaaaaccaaaaa -3′, respectively. The capital letters in ssOND sequences indicate the substituted nucleotides. Both sgRNA and template ssODN were synthesized by Integrated DNA Technologies (IDT, Coralville, IA). Ribonucleoprotein complex consisting of recombinant Cas9 nuclease (IDT) and guide RNA was electroporated into 5×10^5 cells with template ssODN using the Neon system (ThermoFisher Scientific, Waltham, MA). The electroporated cells were transferred to 4 wells of a 96-well plate and cultured in the presence of SCR7 (Cayman Chemical, Ann Arbor, MI; 1533426-72-0) at 1 μM and RS-1 (Calbiochem, San Diego, CA; 553510) at 7.5 μM for 48 hours. The cells were expanded in 20 wells of a 24-

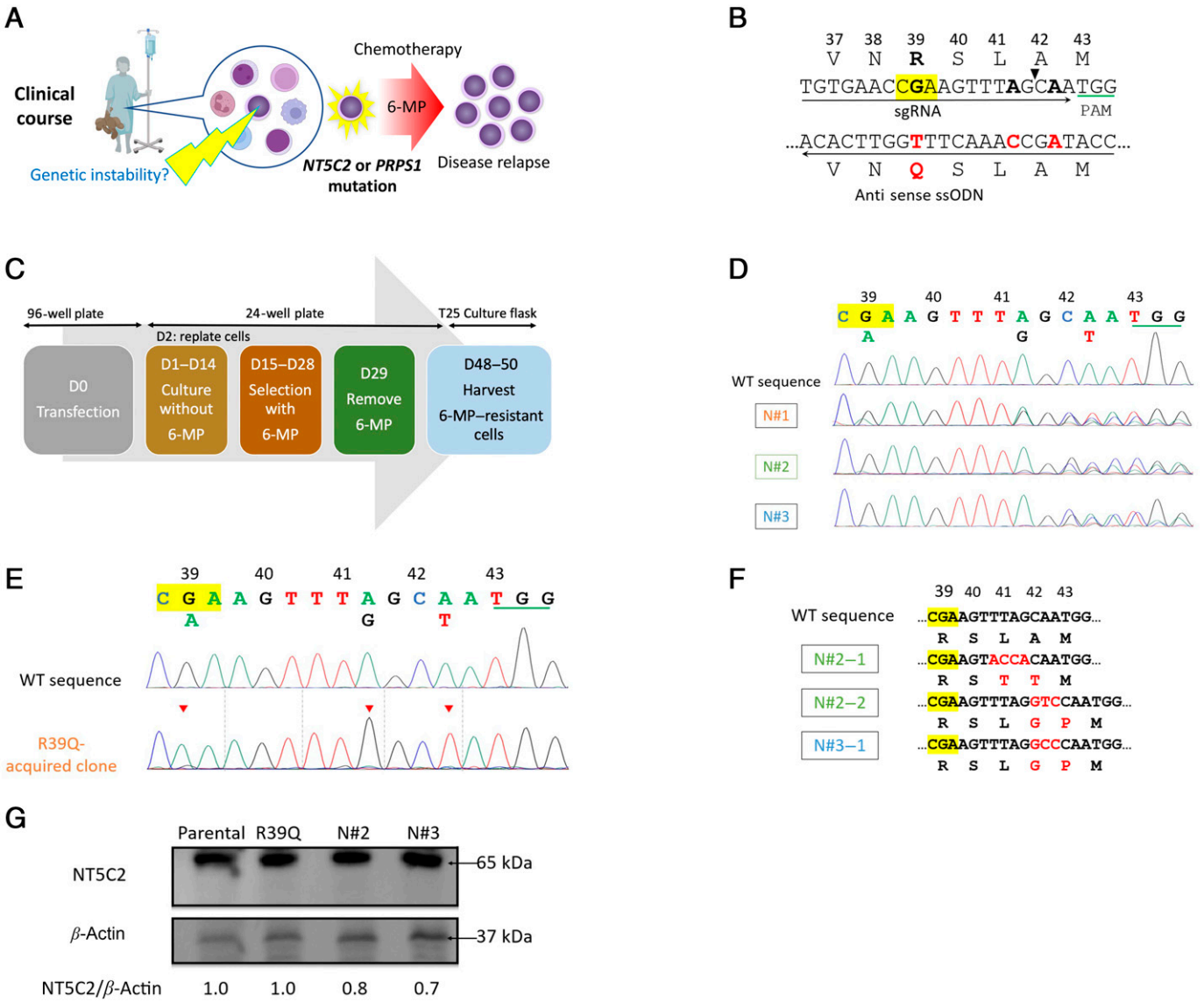

Fig. 1. Introduction of *NT5C2* mutations. (A) The clinical course of early relapse in childhood ALL due to acquisition of *NT5C2* or *PRPS1* mutations by genetic instability during chemotherapy including 6-MP treatment. (B) Schematic diagram of the designed sgRNA and the ssODN. The top two lines indicate wild-type (WT) amino acid and nucleotide sequences, and the bottom two lines indicate mutated nucleotide and amino acid sequences of antisense ssODN. Arrows indicate the directions of sgRNA and ssODN. Targeted codon 39 is highlighted in yellow, and the PAM site is underlined. Black arrowhead indicates the cleave site of Cas9 nuclease. Red characters indicate nucleotide substitutions and the R39Q mutation. (C) Experimental workflow. (D) Sanger sequencing of the genomic PCR products in three *NT5C2*-mutated sublines and parental cells. (E) Sanger sequencing of the genomic PCR product in R39Q-mutated subline. Red arrowheads indicate nucleotide substitutions. (F) Summary of Sanger sequencing of genomic PCR products after TA cloning in *NT5C2*-mutated sublines. Red characters indicate nucleotide substitutions and the resultant amino acid changes. (G) NT5C2 protein expression levels in *NT5C2*-mutated sublines and parental cells. β-Actin expression levels were evaluated as an internal control.

well plate for 2 weeks and then cultured in the presence of 500 nM of 6-MP for 15 days for selection of 6-MP–resistant sublines. For single-cell cloning, parental cells were mixed with subline (25:1), seeded into a U-bottom 96-well plate at a density of 4 cells/100 μl medium per well, expanded for 15 days, and incubated with 6-MP at 500 nM for 11 days.

alamarBlue Cell Viability Assay. Briefly, 2.5 × 104 cells were plated into a 96-well plate in triplicate and cultured in serial concentrations of each agent. Sensitivities to 6-MP (Sigma-Aldrich, St. Louis, MO; 852678) or 6-TG (Sigma-Aldrich; A4882) were tested after 7 days of exposure as previously reported (Somazu et al., 2021). Sensitivities to vincristine (Sigma-Aldrich; 2068-78-2), daunorubicin (Sigma-Aldrich; 30450), dasatinib (a gift from Dr. Tetuzo Tauchi in Tokyo Medical University), mycophenolic acid (MPA) (TokyoChemical Industry, Tokyo, Japan; M2216), and 5-fluorouracil (5-FU) (Enzo Life Sciences, Farmingdale, NY; ALX-480-099-G005) were tested after 72 hours of incubation. The cells were further incubated in the presence of alamarBlue (Bio-Rad Laboratories, Hercules, CA; BUF012A) for 5 hours. Subsequently, absorbance was monitored at 570 nm by a microplate spectrophotometer using 600 nm as a reference wavelength.

Polymerase Chain Reaction. Genomic DNA was extracted using PureLink Genomic DNA Mini Kit (ThermoFisher Scientific) and was amplified by polymerase chain reaction (PCR). Primer sequences were described in Supplemental Table 1. Direct sequencing of each PCR product was performed using each forward primer.

Reverse-Transcription PCR. RNA was extracted using PureLink RNA Mini Kit (ThermoFisher Scientific), and cDNA was synthesized using SuperScript IV Reverse Transcriptase (ThermoFisher

Scientific). Reverse-transcription PCR (RT-PCR) analysis of the *PRPS1* transcript was performed with forward primer in exon 1 and reverse primer in exon 4 of the *PRPS1* gene. Real-time RT-PCR analysis of the *PRPS1* gene was performed using Taqman Probe Kit (IDT; Hs.PT.58.192794749) with *ACTB* gene expression level (ThermoFisher Hs99999903_m1) as an internal control.

TA Cloning. Genomic PCR and RT-PCR products were cloned using a TOPO TA Cloning Kit (Invitrogen, Waltham, MA). For each PCR product, plasmid DNA was extracted from 5–10 colonies using the QIA Plasmid Mini kit (Qiagen, Germantown, MD) and subjected to direct sequencing.

Droplet Digital PCR. We incubated KOPN55bi cells with 6-MP at 100, 200, or 500 nM for 1–4 weeks and extracted genomic DNA. The droplet digital PCR (ddPCR) was performed using a Droplet Digital PCR QX200 system (Bio-Rad Laboratories, Hercules, CA) according to the manufacturer's instructions. The mutation detection assays for *NT5C2*-R39Q and *PRPS1*-S103N were purchased from Bio-Rad. 100 ng of DNA was added to a 20-μL PCR mixture containing HaeIII restriction enzyme, and droplet generation was carried out using a Droplet Generator (Bio-Rad). PCR amplification was performed in the following conditions: denaturing at 95°C for 10 minutes, 40 cycles of PCR at 94°C for 30 seconds and 56°C for 2 minutes, and a final extension at 98°C for 10 minutes. PCR-positive and PCR-negative droplets were counted using the QX200 droplet reader (Bio-Rad), and the threshold for each assay was determined by comparing wild-type and no-template ddPCR results. All experiments were performed in triplicate.

Flow Cytometric Analysis. To evaluate cellular ABCC4 expression levels, after fixation and permeabilization with BD Cytofix/Cytoperm Fixation/Permeabilization Kit (BD, Franklin Lakes, NY; 554714), the cells were stained with anti-ABCC4 antibody (Cell signaling, Beverly, MA; D2Q2O) (1:100) or mouse IgG (Beckman Coulter, Brea, CA; IM2475) (1:1000), subsequently with Alexa Flour 488–conjugated goat anti-rabbit IgG (ThermoFisher Scientific; A-11008) (1:1000) as the second antibody, and then processed for flow cytometry (FACSCalibur; BD). To detect apoptotic cell death, cells were stained with Annexin–fluorescein isothiocyanate and phosphatidylinositol [Medical & Biologic Laboratories (MBL), Nagoya, Japan] and analyzed by flow cytometry.

Western Blot Analysis. Cells were solubilized in lysis buffer (50 mM Tris-HCl, pH 7.5; 150 mM NaCl; 1% Nonidet P-40; 5 mM EDTA; 0.05% NaN3; 1 mM phenylmethylsulfonyl fluoride; 100 μM sodium vanadate) on ice. The cell lysates were separated on an SDS polyacrylamide gel under reducing conditions and transferred to a nitrocellulose membrane. Each membrane was incubated with anti-NT5C2 (Abcam, Cambridge, MA; ab96084), anti-PRPS1 (Proteintech, Tokyo, Japan; 15549-1-AP), anti–β-actin (MBL; PM053-7), and anti–α-tubulin (Sigma-Aldrich; T5168) antibodies at 4°C overnight. Subsequently, the membranes were incubated with horseradish peroxidase–labeled anti-mouse or anti-rabbit IgGs (MBL) at room temperature for 1 hour. Then, the blots were developed using an enhanced chemiluminescence detection kit (GE Healthcare, Little Chalfont, Buckinghamshire, UK). The band density was semiquantified using Image J (National Institutes of Health, Bethesda, MD).

Quantification of Intracellular Thioinosine Monophosphate, Thioguanine Nucleotide, and DNA-thioguanin. For the measurement of thioinosine monophosphate (TIMP), cells were incubated with 6-MP at 10 μM for 4 hours or at sequential concentrations according to pharmacokinetics. The cells were washed with cold PBS and then centrifuged to collect the cell pellets. Cell pellets were frozen at −80°C overnight. After thawing, the samples were resuspended in 180 μl of 80% methanol, vortexed, and then kept on ice for 10 minutes. These suspensions were centrifuged for 10 minutes at 10,000*g*. The supernatants were filtrated and measured by combining liquid chromatography with tandem mass spectrometry (LC-MS/MS) with InertSustain AQ-C18 PEEK column (1.9 μm, 2.1 × 100 mm; GL Sciences, Tokyo, Japan). For the measurement of thioguanine nucleotide (TGN), cells were incubated with 6-MP at 500 nM for 5 days. After washing with PBS, pellets of the cells were resuspended in 200 μl of water and frozen at −80°C overnight. After thawing, the cell pellets were sonicated for 20 seconds and resuspended in 100 μl of 25 mmol/L dithiothreitols (Kanto Chemical, Tokyo, Japan), 5 μl of 125 μM thioguanine-13C2, 15N (Toronto Research Chemicals, North York,, ON, Canada) as internal standard, and 20 μl of 60% perchloric acid (Kanto Chemical, Tokyo, Japan). After centrifugation for 10 minutes at 13,000*g*, the supernatants were incubated for 1 hour at 95°C. Thioguanine concentrations were measured by LC-MS/MS with CORTECS C18+ column (1.6 μm, 2.1 × 50 mm; Waters, Milford, MA). For the measurement of DNA-thioguanin (DNA-TG), cells were incubated with 6-MP at 500 nM for 2 days. DNA was extracted using PureLink Genomic DNA Mini Kit (ThermoFisher Scientific). The DNA samples with the addition of 6-methylmercaptopurine-d3 (Toronto Research Chemicals) as an internal standard were denatured at 100°C for 5 minutes and digested by 0.6 U nuclease P1 from *Penicillium citrinum* (Sigma-Aldrich) with a digestive buffer (500 mM sodium acetate, 10 mM MgCl2 pH 5.3) for 1 hour at 50°C. The digested DNA was treated with 3 U of calf intestinal alkaline phosphatase in the presence of reaction buffer (Toyobo, Osaka, Japan) at 37°C for 30 minutes, then deoxy thioguanosine was measured by LC-MS/MS with CORTECS C18+ column (1.6 μm, 2.1 × 50 mm; Waters). The analyses were performed in triplicate.

Statistics. Dose-response curves to be fit by nonlinear regression and IC_{50} values were determined by R software version 4.2.2 with the "drc" package. Subsequently, the IC_{50} values were automatically determined by the R software based on the four-parameter log-logistic function model as follows: Y = Low CI + (High CI-Low CI)/[1 + 10 ^ (Log IC_{50}-X)]; Low CI: the minimum cell index values; High CI: the maximum cell index values; Y: Cell viability; X: the log of concentration. Each IC_{50} value as well as cell viability indicated the representative value in the multiple experiments (at least three independent analyses). One-way ANOVA followed by Dunnett's multiple comparison test was performed using R software. We used the zero-interaction potency (ZIP) model, in which the combined effect of two drugs is captured by comparing the changes in the potency of the dose-response curves between each individual drug and their combinations since it provides an improved solution for identifying true synergistic interactions with a relatively low false positive rate (Yadav et al., 2015; Zheng et al., 2022). The ZIP model evaluates the delta scores, which are deviations from the expectation of zero interaction for synergistic effect, and performs the z-tests, which compare the distribution of delta scores calculated by interactive bootstrap resampling of the model's parameter space to 0. The resulting two-drug-specific *P* value is used to reject or accept the null hypothesis. The combination effect is defined as follows: synergy score > 10: synergistic effect; −10 < synergy score < 10: additive effect; synergy score < −10: antagonistic effect. We also applied the Loewe additivity model, which defines the expected effect as if a drug is combined with itself by calculating the combination index with CalcuSyn software as follows: combination index = (D)1/(Dx)1 + (D)2/(Dx)2 + (D)1(D)2/(Dx)1(Dx)2, where: (Dx)1 or (Dx)2 is the dose of Drug 1 or Drug 2 as a single agent required to produce an X% effect; (D)1 or (D)2 is the dose of Drug 1 or Drug 2 required to produce the same X% effect in the combination of two drugs. The combination effect is defined as follows: combination index < 1: synergistic effect; combination index = 1: additive effect; combination index > 1: antagonistic effect.

Results

Introduction of *NT5C2* Mutations Using the CRISPR/Cas9 System. Among four hotspot mutations of the *NT5C2* gene (R39Q, R238W/L/G/Q, R367Q, and D407A/Y/E/H) (Dieck et al., 2018; Dieck and Ferrando, 2019), an appropriate protospacer adjacent motif (PAM) site with a high off-target score was available in the adjacent region of codon 39 but not codons 238, 367, and 407. Thus, we tried to introduce the R39Q mutation of the *NT5C2* gene into a human lymphoid leukemia

cell line by HR using the CRISPR/Cas9 system. We designed sgRNA targeting at the PAM site located 10 bp away from codon 39 (Fig. 1B). As the repair template, ssODN with 100 nucleotides complementary to the non-target strand (antisense) was used as a repair template. The ssODN contained a R39Q mutation (cga > cAa) and two silent mutations to avoid recutting the repaired loci (Fig. 1B). We used KOPN55bi as the target cell line, which was established from a patient with lymphoid crisis of chronic myeloid leukemia. KOPN55bi is highly resistant to olaparib, a Poly (ADP)-ribose polymerase 1 (PARP1) inhibitor, suggesting that the DNA repair system for HR is active (Tamai et al., 2018). KOPN55bi has no mutation in the *NT5C2* and *PRPS1* genes (at least in the coding region), and it has a wild-type genotype of *NUDT15* polymorphism (Somazu et al., 2021). Parental KOPN55bi was highly sensitive to 6-MP in vitro in the 7-day incubation assay (Somazu et al., 2021).

To introduce R39Q mutation by HR, the ribonucleoprotein complex consisting of sgRNA and Cas9 was electroporated into KOPN55bi cells with the ssODN. To enhance HR efficiency, we treated the cells with RS-1 and SCR7. RS-1 is a stimulator of RAD51, a key component in the HR repair pathway (Song et al., 2016), whereas SCR7 is an inhibitor for DNA-ligase IV, which is involved in the NHEJ repair pathway (Maruyama et al., 2015). Transfected cells were incubated in 4 wells of a 96-well plate with 1 μM of SCR7 and 7.5 μM of RS-1 for 48 hours, then transferred to 20 wells of a 24-well plate (Fig. 1C). After 14 days of expansion, the cells were incubated with 6-MP at 500 nM, which is equivalent to the serum C_{max} level during maintenance therapy, for 15 days. Subsequently, the cells were cultured in the absence of 6-MP. Three weeks after 6-MP selection, 6-MP–resistant sublines were expanded in all 20 wells and were then transferred to culture flasks for further experiments (Fig. 1C). We further analyzed three representative sublines.

In direct sequencing of the genomic PCR products, each subline was a mixture of heterogeneous populations with overlapping traces in a chromatogram (Fig. 1D). Since the R39Q mutation was partly confirmed in subline N#1, we performed single-cell cloning by serial dilution. In the obtained clone, homozygous R39Q mutation and two intended silent mutations were confirmed (Fig. 1E), indicating that R39Q mutation was induced as a result of HR. Considering that 6-MP treatment of selection may induce R39Q mutation, we performed ddPCR analysis in the parental cells treated with 6-MP at 100 nM, 200 nM, or 500 nM for 1, 2, or 4 weeks (Supplemental Table 2). The overall incidence of R39Q mutation was less than 0.011%, and the incidence of R39Q mutation after 2-week incubation with 500 nM of 6-MP, which was almost identical to the condition for selection, was 0.011%. We also performed Sanger sequencing of the coding regions of the *NT5C2* gene and confirmed no additional unintended mutations (Supplemental Fig. 1A). In addition, we simply performed direct Sanger sequencing of the genomic PCR products at three possible off-target sites located in the *LCORL*, *RTTN*, and *IGFBP3* genes, which were predicted by the sgRNA design software. No clear mutations were observed in these sites of the genomic DNA extracted from the subline compared with those extracted from the parent cells. (Supplemental Fig. 2A). These observations indicated that R39Q mutation was induced as a result of HR without any notable off-target effect.

Using two other sublines (N#2 and N#3), we performed Sanger sequencing of genomic PCR products after TA cloning (Fig. 1F; Supplemental Fig. 3). Each sequence indicated in-frame mutation due to small insertion/deletions (indels) at the double-strand break site. As a result, Leu^{41}-Ala^{42} residues would be substituted to Thr-Thr, Leu-Gly-Pro. We finally evaluated NT5C2 protein expression levels in the R39Q subline and sublines N#2 and N#3 by western blot analysis using β-actin expression as an internal control (Fig. 1G). We confirmed similar NT5C2 expression levels in each *NT5C2*-mutated subline and the parental cells.

Introduction of *PRPS1* Mutation by the CRISPR/Cas9 System. We next tried to introduce relapse-specific mutations of the *PRPS1* gene. A190T/V and S103N mutations are common hotspot mutations (Li et al., 2015), and the appropriate PAM site with a high off-target score was available for codon 103 but not for codon 190; thus, we chose the *PRPS1*-S103N mutation as a target. We designed sgRNA targeting at the PAM site adjacent to the S103 codon (Fig. 2A). The antisense ssODN contained the S103N mutation (agc > aAc) and one silent mutation at the PAM motif to prevent the recutting of repaired loci. We performed the same workflow of introducing *NT5C2* mutation (Fig. 1B) and obtained 6-MP–resistant sublines in 12 out of 20 wells. We further analyzed five representative sublines. Subline P#1 showed the homozygous S103N mutation with the designed silent mutation in the direct sequencing of genomic PCR product (Fig. 2B), indicating that S103N mutation was induced as a result of HR. In the ddPCR analysis (Supplemental Table 2), the overall incidence of S103N mutation was less than 0.037%, and the incidence after 2-week incubation with 500 nM of 6-MP was 0.005%. Additionally, in the Sanger sequencing of the coding regions of the *PRPS1* gene, no additional unintended mutation was observed (Supplemental Fig. 1B). Moreover, direct sequencing of the genomic PCR products at three possible off-target sites located in the *FGGY*, *NCK2*, and *NHSL1* genes revealed no clear mutations in these sites (Supplemental Fig. 2B). These observations indicated that S103N mutation was induced as a result of HR without any notable off-target effect.

Subline P#2 showed the heterozygous S103T mutation in combination with homozygous 3-bp insertion (Supplemental Fig. 4A). Sublines P#3, P#4, and P#5 showed overlapping traces in the direct sequencing of the genomic PCR products. Thus, we performed Sanger sequencing of genomic PCR products after TA cloning (Fig. 2C; Supplemental Fig. 4, B–E). In subline P#3, five types of 3-bp insertion were observed at the target site (Fig. 2C; Supplemental Fig. 4, B and C), which would result in the insertion of Gly (GGG or GGC), Ala (GCT or GCC), or Ser (TCG). In subline P#4, 6-bp insertion of "CCCCCC," which would result in the insertion of Pro-Pro, was observed (Fig. 2C; Supplemental Fig. 4D). Furthermore, in subline P#4, the substitution of "tttag/AGC" to "cccag/CTC" was observed at the intron 2/exon 3 boundary (Fig. 2C; Supplemental Fig. 4E). In this mutation, in spite of the mutation at the 3′ end of intron 2, the "ag" consensus of splicing site was conserved. Consistently, in the Sanger sequencing of RT-PCR products after TA cloning, the corresponding substitution of "AGC" to "CTC" at codon 103, which would result in the transition of Ser to Leu, was confirmed. In one of the genomic sequences of subline P#5, the substitution of "atttag" to "ccaaca" was observed at the 3′ end of intron 2, which completely disrupted the splicing acceptor consensus sequence (Fig. 2D; Supplemental Fig. 4F). Consistently, in the Sanger sequencing of the RT-PCR products after TA-cloning,

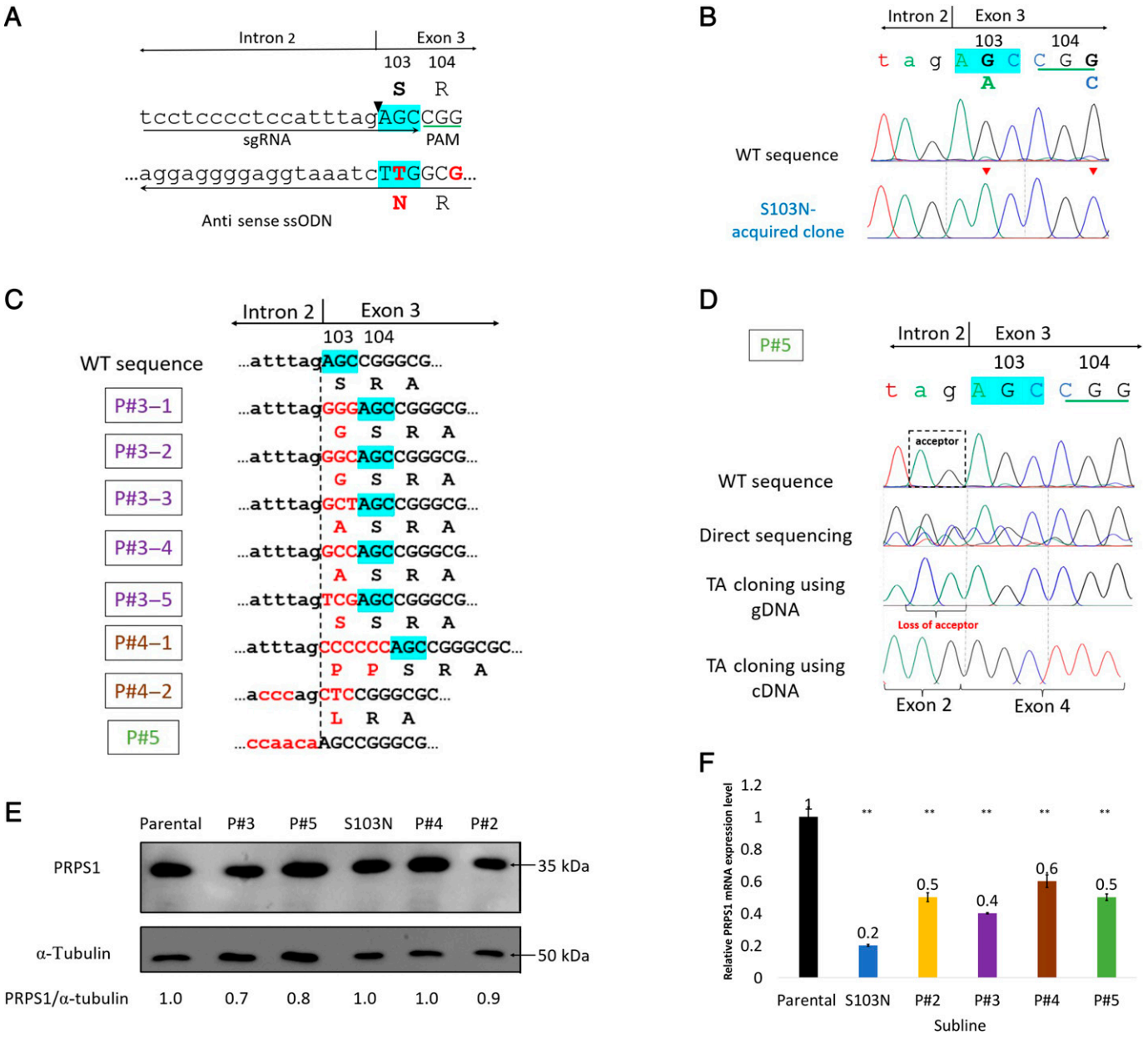

Fig. 2. Introduction of *PRPS1* mutations. (A) Schematic diagram of the sgRNA and the ssODN. Intron 2–exon 3 boundary was indicated at the top of the panel. The top two lines indicate wild-type (WT) amino acid and nucleotide sequences, and the bottom two lines indicate mutated nucleotides and amino acid sequences of antisense ssODN. Arrows indicate the directions of sgRNA and ssODN. Targeted codon 103 is highlighted in blue, and the PAM site is underlined. Black arrowhead indicates the cleave site of Cas9 nuclease. Red characters indicate nucleotide substitutions and the S103N mutation. (B) Sanger sequencing of the genomic PCR product in S103N mutated subline. Red arrowheads indicate nucleotide substitutions. (C) Summary of Sanger sequencing of genomic PCR products after TA cloning in *PRPS1*-mutated sublines. Red characters indicate nucleotide substitutions and the resultant amino acid changes. The dashed line indicates the intron 2–exon 3 boundary. (D) Sanger sequencing of genomic PCR and RT-PCR products after TA cloning in subline P#5. Dash boxes indicate the splice acceptor site. (E) PRPS1 protein expression levels in *PRPS1*-mutated sublines and parental cells. α-Tubulin expression levels were evaluated as an internal control. (F) PRPS1 mRNA expression levels in *PRPS1*-mutated sublines and their parental cells. The vertical axis indicates the relative mRNA expression levels. Error bars indicate the standard deviations of triplicated analysis (**$P < 0.01$; one-way ANOVA followed by Dunnett's test).

we confirmed the corresponding sequence, in which exon 2 was directly fused to exon 4. We finally evaluated PRPS1 protein expression levels in the S103N subline and the sublines P#2-5 by western blot analysis using α-tubulin expression as the internal control (Fig. 2E). Although there were certain variations among sublines, relative PRPS1 protein expression levels in the five representative sublines were almost identical or relatively lower than those in the parental cells. Thus, we further evaluated *PRPS1* gene expression levels by real-time PCR (Fig. 2F) and confirmed the remarkably lower expression in the *PRPS1*-mutated sublines than in the parental cells.

***NT5C2* and *PRPS1* Mutations Confer Thiopurine Resistance.** We recently demonstrated that the continuous 7-day-exposure assay is pharmacologically useful to evaluate the significance of the *NT5C2* and *PRPS1* mutations in

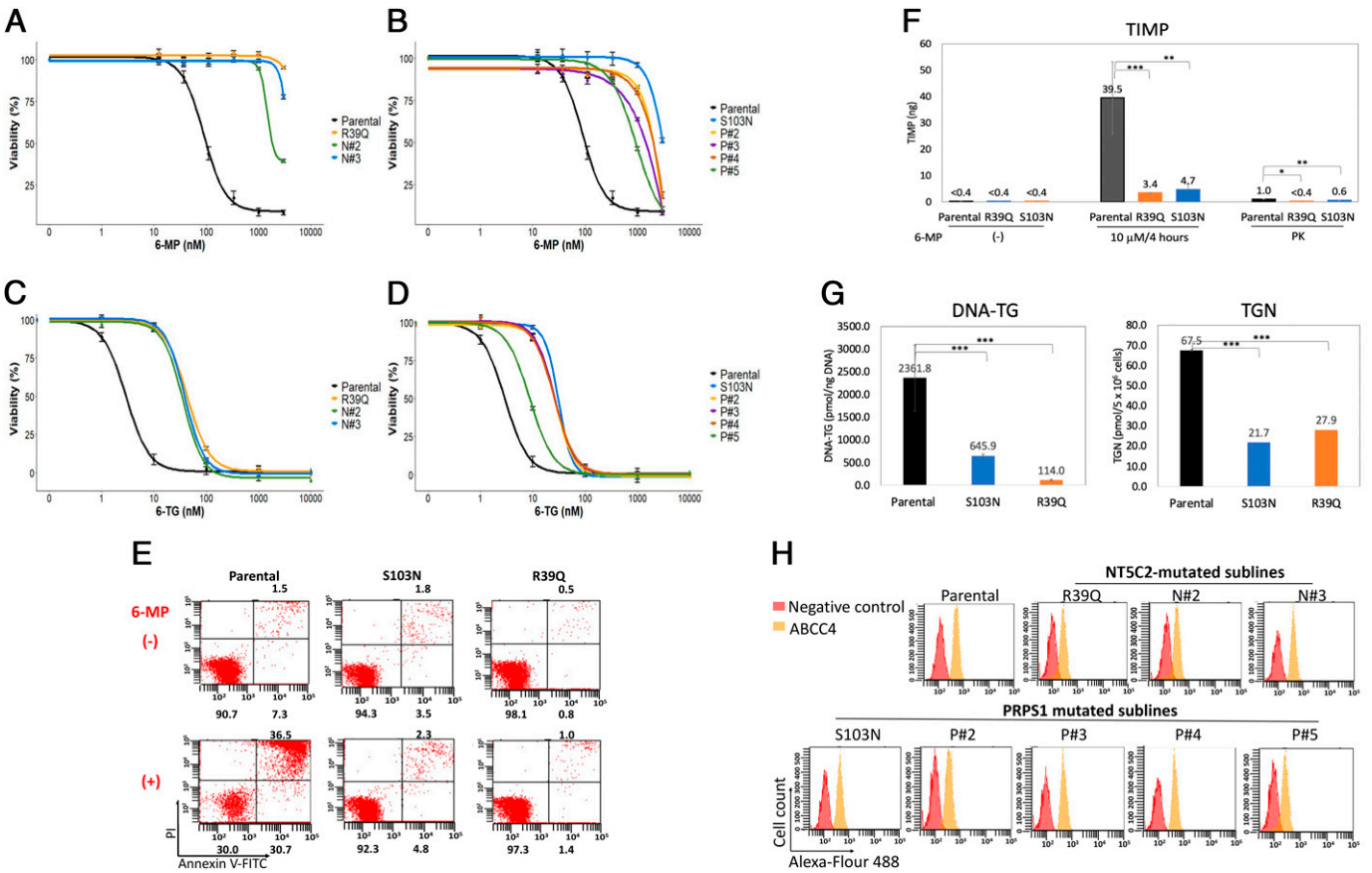

Fig. 3. Thiopurine resistance in the *NT5C2* and *PRPS1*-mutated sublines. (A–D) Dose-response curves of 6-MP (A and B) and 6-TG (C and D) in the *NT5C2* (A and C) or *PRPS1*-mutated sublines (C and D) and parental cells. Horizontal and vertical axes indicate the concentrations of 6-MP or 6-TG and cell viability in the alamarBlue assay, respectively. Error bars indicate the standard deviations of triplicated analysis. (E) Induction of apoptosis after 7-day exposure to 200 nM of 6-MP in *NT5C2*-R39Q and *PRPS1*-S103N–mutated sublines and parental cells. Flow cytometric analysis of annexin V binding (horizontal axis) and phosphatidylinositol (PI) staining (vertical axis) are indicated. The percentages of living cells (lower left), early apoptotic cells (lower right), and late apoptotic cells (upper right) are indicated in the corner of each panel. (F) Intracellular TIMP levels in the *NT5C2*-R39Q (orange column) and *PRPS1*-S103N–mutated (blue column) sublines and parental cells (gray column) after continuous exposure to 10 μM of 6-MP for 4 hours (middle panel) and sequential exposure to 600 nM of 6-MP for 1.3 hours, 300 nM for 1.3 hours, and 150 nM for 3.3 hours (left panel). Error bars indicate the standard deviations of triplicated analysis (*$P < 0.05$; **$P < 0.01$; ***$P < 0.05$; one-way ANOVA followed by Dunnett test). (G) Intracellular DNA-TG and TGN levels in the *NT5C2*-R39Q (orange column) and *PRPS1*-S103N (blue column) sublines and parental cells (gray column) after exposure to 6-MP. Error bars indicate the standard deviations of triplicated analysis (***$P < 0.001$; one-way ANOVA followed by Dunnett test). (H) Cellular ABCC4 expression levels in *NT5C2* and *PRPS1*-mutated sublines and parental cells. Flow cytometric analysis of Alexa Flour 488 staining (horizontal axis) and cell count (vertical axis) are indicated. Red and orange shades indicate isotype control and anti-ABCC4 antibody fluorescence intensities, respectively. FITC, fluorescein isothiocyanate.

thiopurine sensitivity (Somazu et al., 2021). We first evaluated 6-MP sensitivity after 7-day exposure using the alamarBlue assay. Parental KOPN55bi cells were sensitive to 6-MP (Fig. 3A). The IC_{50} value of 6-MP in the parental cells was 107 nM, which was approximately five times lower than the clinical serum C_{max} level (approximately 560 nM) during maintenance therapy (Balis et al., 1998). In contrast, three *NT5C2*-mutated and five *PRPS1*-mutated sublines were highly resistant to 6-MP (Fig. 3, A and B). The IC_{50} values of 6-MP in the *NT5C2* and *PRPS1*-mutated sublines were higher than 1000 nM, which was higher than the C_{max} concentration of 6-MP during maintenance therapy. We next evaluated sensitivity to 6-TG after 7-day exposure using alamarBlue assay (Fig. 3, C and D). Similar to 6-MP sensitivity, the parental cells were sensitive to 6-TG, whereas the *NT5C2* and *PRPS1*-mutated sublines were remarkably more resistant. The IC_{50} of 6-TG in the parental cells was 3.0 nM, which was approximately 100 times lower than the C_{max} level of 6-TG (317 nM) during daily oral administration in childhood ALL patients (Lennard et al., 1993). In contrast, the IC_{50} values of 6-TG in the *NT5C2* and *PRPS1*-mutated sublines were approximately 10 times higher than those in the parental cells. We further evaluated the induction of apoptosis after 7-day exposure to 6-MP at 200 nM by flow cytometry (Fig. 3E; Supplemental Fig. 5). Approximately half of the parental cells underwent apoptosis, whereas most of the *NT5C2* or *PRPS1*-mutated sublines survived.

6-MP is a prodrug that is converted to TIMP via the purine synthesis de novo pathway. TIMP is finally metabolized to 6-thioguanosine 5′-triphosphate, which is incorporated into DNA and reveals antileukemic activity (Karran and Attard, 2008). Thus, we measured the intracellular levels of TIMP in the *NT5C2*-R39Q and *PRPS1*-S103N sublines as well as the parental cells after exposure to 6-MP using liquid chromatography-mass spectrometry (LC-MS) (Fig. 3F). We investigated 2 different exposure conditions as follows: one was continuous exposure to 10 μM for 4 hours based on the previous report (Li et al., 2015), whereas the other was sequential exposure to 600 nM for 1.3 hours, 300 nM for 1.3 hours, and 150 nM for 3.3 hours based on the pharmacokinetics of 6-MP during the

maintenance therapy (Balis et al., 1998). After continuous exposure, intracellular TIMP levels of the parental cells (mean ± S.D.; 39.5 ± 13.6 ng) were higher than those of the *NT5C2*-R39Q subline (3.4 ± 0.1 ng, $P < 0.001$ in Dunnett's test) and the *PRPS1*-S103N subline (4.7 ± 1.9 ng, $P < 0.01$). Moreover, after pharmacological exposure, intracellular TIMP levels of parental cells (1.0 ± 0.1 ng) were also ly higher than those of the *NT5C2*-R39Q subline (< 0.4 ng, $P < 0.05$) and the *PRPS1*-S103N subline (0.6 ± 0.1 ng, $P < 0.01$).

We next measured levels of cellular TGN, which is one of the active 6-MP metabolites, and DNA-TG, which is the active 6-MP metabolites incorporated into DNA, in the *NT5C2*-R39Q and *PRPS1*-S103N sublines as well as the parental cells treated with 6-MP at 500 nM for 5 days (TGN) or 2 days (DNA-TG). Cellular TGN levels of the parental cells (67.5 ± 0.5 pmol/5 × 10^6 cells) were ly higher than those of the *NT5C2*-R39Q (27.9 ± 4.3 pmol/5 × 10^6 cells, $P < 0.001$ in Dunnett's test) and the *PRPS1*-S103N sublines (21.6 ± 0.9 pmol/5 × 10^6 cells, $P < 0.001$) (Fig. 3G). Similarly, the DNA-TG levels of the parental cells (2362 ± 1269 pmol/ng DNA) were ly higher than those of the *NT5C2*-R39Q (114 ± 28 pmol/ng DNA, $P < 0.001$) and the *PRPS1*-S103N sublines (646 ± 73 pmol/ng DNA, $P < 0.001$) (Fig. 3G). These observations indicated that thiopurine resistance in *NT5C2*-R39Q and *PRPS1*-S103N sublines was associated with the reduction in the levels of intracellular TIMP, TGN, and DNA-TG.

In the present study, during the selection of mutated sublines, the cells were exposed to 500 nM of 6-MP for 15 days. Thus, the obtained sublines might also acquire other thiopurine resistance mechanisms. In this context, since drug efflux by ABCC4 is reportedly involved in the thiopurine resistance of leukemia cells (Peng et al., 2008), we evaluated the cellular expression levels of ABCC4 by flow cytometry. Although there were certain levels of variability among *NT5C2*-mutated and *PRPS1*-mutated sublines, ABCC4 expression levels in these sublines were almost similar to that in parental cells (Fig. 3H). These observations suggested that the upregulation of ABCC4 is unlikely to be involved in the thiopurine resistance in the obtained sublines.

Next, we evaluated the sensitivity to other chemotherapeutic agents in the *NT5C2* and *PRPS1*-mutated sublines using

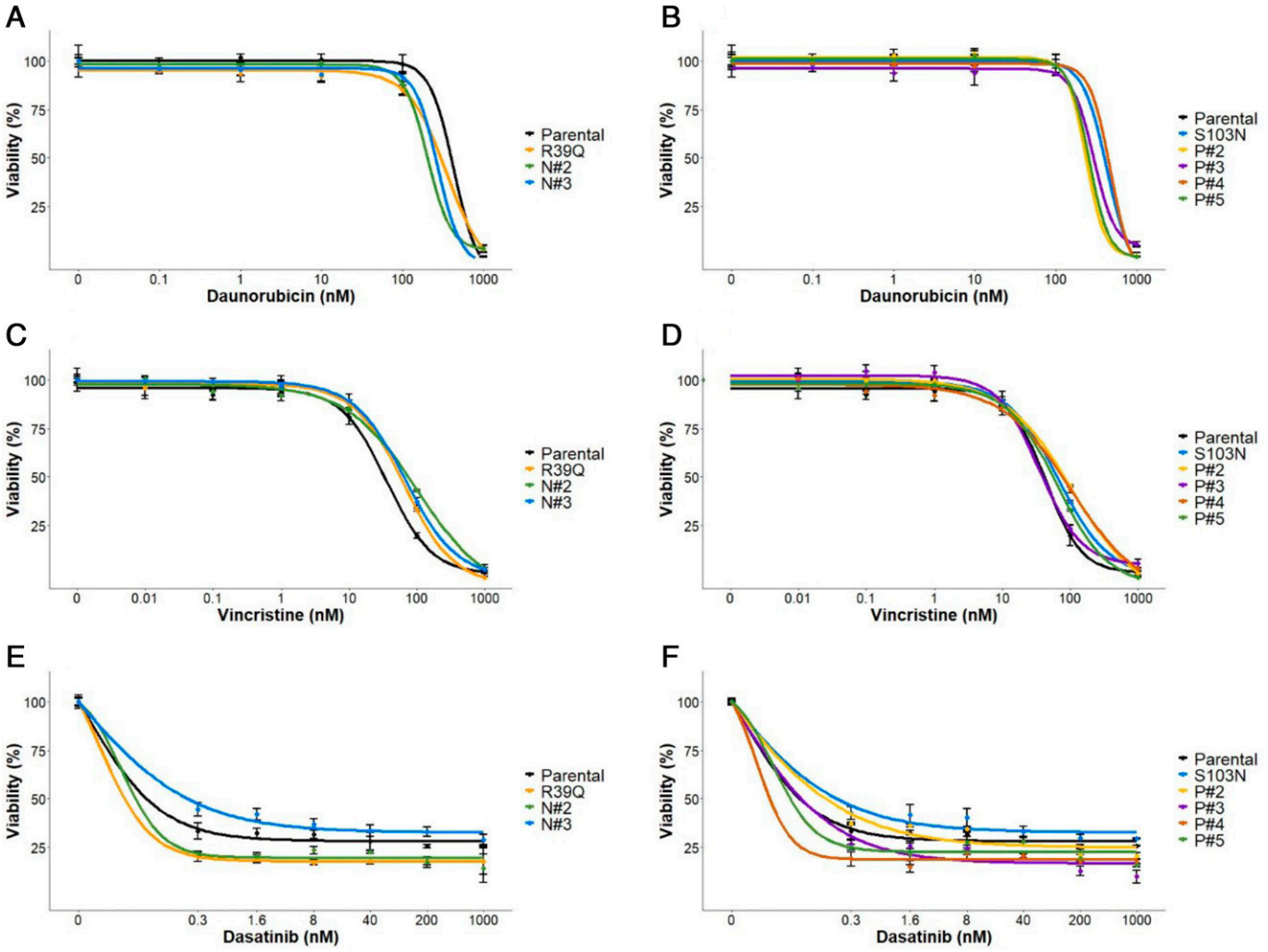

Fig. 4. Sensitivities to chemotherapeutic agents in the *NT5C2* and *PRPS1*-mutated sublines. Dose-response curves of daunorubicin (A and B), vincristine (C and D), and dasatinib (E and F) in the *NT5C2* (A, C and E) and *PRPS1*-mutated sublines (B, D and F) and parental cells (black line). Horizontal and vertical axes indicate the concentrations of each agent and cell viability, respectively. Error bars indicate the standard deviations of triplicated analysis.

alamarBlue assay. We investigated the sensitivities to daunorubicin (Fig. 4, A and B) and vincristine (Fig. 4, C and D) and confirmed similar sensitivities in the *NT5C2* and *PRPS1*-mutated sublines and parental cells. We also evaluated the sensitivity to dasatinib since KOPN55bi is a Ph^+ lymphoid leukemic cell line. The dasatinib sensitivities in the *NT5C2*-mutated and *PRPS1*-mutated sublines were almost similar to those in the parental cells (Fig. 4, E and F). These results indicated that the *NT5C2* and the *PRPS1*-mutated sublines showed thiopurine-specific resistance.

Overcoming Drug Resistance Due to *NT5C2* or *PRPS1* Mutations. Considering that all of the three *NT5C2*-mutated sublines showed thiopurine-specific resistance, these gain-of-function mutations of the *NT5C2* gene may enhance the dependency of leukemia cells on de novo purine synthesis. MPA is an inosine monophosphate dehydrogenase (IMPDH) inhibitor that reportedly shows antitumor activity by blocking de novo purine synthesis (Tzoneva et al., 2018; Naffouje et al., 2019). Thus, we investigated the antileukemic activity of MPA in the *NT5C2*-mutated sublines using alamarBlue assay (Fig. 5A). The *NT5C2*-mutated sublines were remarkably more sensitive to MPA than the parental cells.

We next evaluated the induction of apoptosis after 72-hour exposure to MPA at 1 μM, which is almost consistent with serum MPA level during oral administration at the therapeutic dose (Ferreira et al., 2020) (Fig. 5B). In the parental cells, 65% of the MPA-treated cells underwent apoptosis, whereas in three *NT5C2*-mutated sublines, approximately 80% of the MPA-treated cells underwent apoptosis. These observations demonstrated that the *NT5C2* mutation intensified the sensitivity of leukemia cells to MPA at therapeutic concentration.

We further investigated the synergistic activity of MPA with 6-MP since a previous report revealed synergy in the T cell–ALL cell line (Wang et al., 2018). We treated the *NT5C2*-R39Q subline with both MPA and 6-MP at wide ranges of concentrations, and synergistic activities were evaluated based on the results of alamarBlue assay (Fig. 5, C and D; Supplemental Table 3). To evaluate the synergistic effect, we applied two models: the ZIP model and the Loewe model. When synergy scores were calculated based on the ZIP model, the highest synergy score (41.7, $P = 0.025$ in the z-test) was observed between MPA at 312 nM, which was within the therapeutic serum concentration level of MPA, and 6-MP at 3000 nM, which was approximately 5 times higher than the serum C_{max} level of 6-MP; cell viabilities were markedly decreased from 93.1% (MPA alone) and 86.9% (6-MP alone) to 39.6% (in combination). When the Loewe additivity model was applied, the combination index was 0.36, thus indicating a synergistic effect. However, a synergistic effect was not observed between therapeutic concentrations of MPA (1250 nM) and 6-MP (333 nM); cell viabilities were slightly decreased from 34.2% (MPA alone) and 100% (6-MP alone) to 30.5% (in combination), and the synergy score and combination index were 2.3 ($P = 0.7$) and 1.0, respectively.

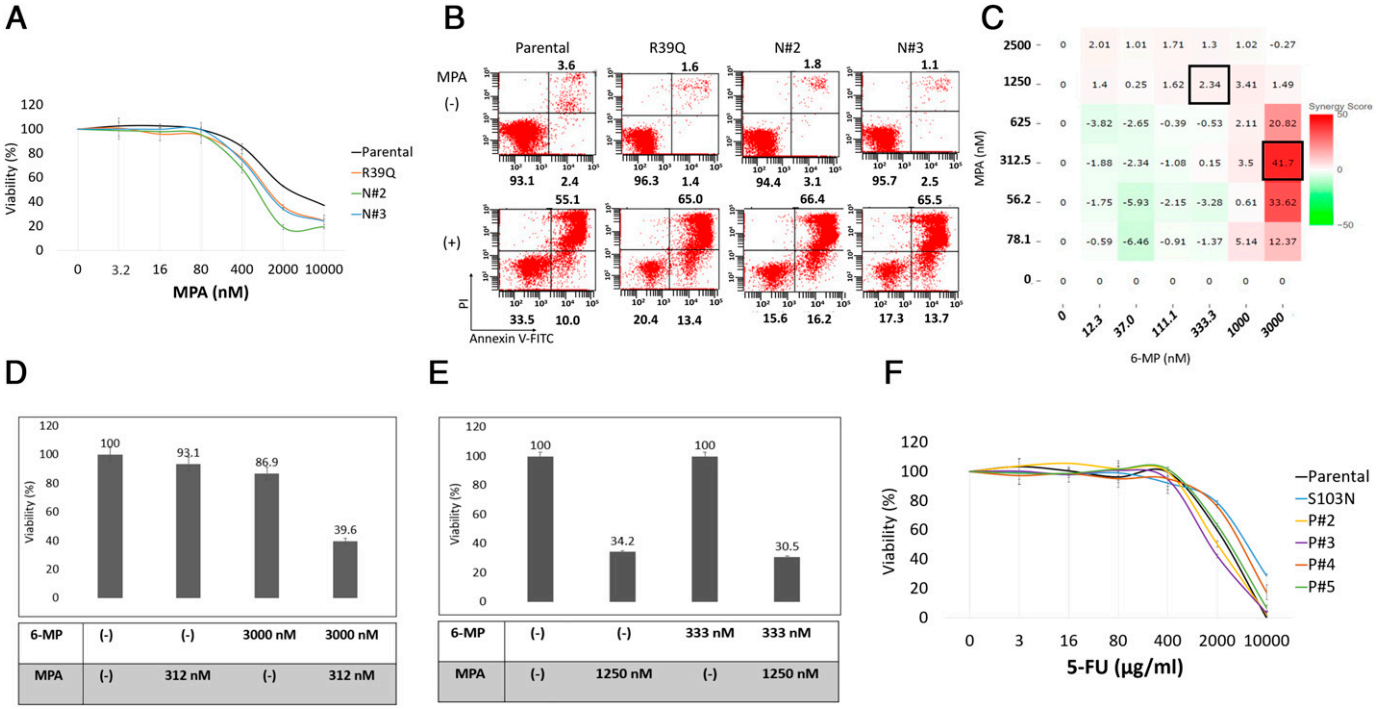

Fig. 5. Overcoming thiopurine resistance in the *NT5C2* and *PRPS1*-mutated sublines. (A) Dose-response curves of MPA sensitivity in *NT5C2*-R39Q subline and parental cells (black line). Horizontal and vertical axes indicate the concentrations of MPA and cell viability, respectively. Error bars indicate standard deviations in triplicated analysis. (B) Induction of apoptosis after 3-day exposure to 1 μM of MPA in *NT5C2*-mutated sublines and parental cells. Flow cytometric analysis of annexin V binding (horizontal axis) and phosphatidylinositol (PI) staining (vertical axis) are indicated. The percentages of living cells (lower left), early apoptotic cells (lower right), and late apoptotic cells (upper right) are indicated in the corner of each panel. (C and D) Cell viability of the *NT5C2*-R39Q subline under treatment of 6-MP at 3000 nM and MPA at 312.5 nM (C) or 6-MP at 333.3 nM and MPA at 1250 nM (D). Error bars indicate standard deviations in triplicated analysis. (E and F) Combination effect of MPA and 6-MP in *NT5C2*-R39Q subline. Each synergy score determined by SynergyFinder software (E) and combination index determined by CalcuSyn software (F) at diverse concentrations is indicated. Boxes indicate the combinations demonstrated in the following figures. (G) Dose-response curves of 5-FU in the *PRPS1*-mutated sublines and parental cells (black line). Horizontal and vertical axes indicate the concentrations of 5-FU and cell viability, respectively. Error bars indicate the standard deviations in triplicated analysis. FITC, fluorescein isothiocyanate.

We next investigated the antileukemic activity of 5-FU in the *PRPS1*-mutated sublines since it has been reported that ALL cell lines transduced with mutated *PRPS1* cDNA were more sensitive to 5-FU than those with wild-type cDNA (Wang et al., 2018). We evaluated the sensitivity to 5-FU using alamarBlue assay (Fig. 5G). The IC_{50} value of 5-FU in the parental cells was approximately 2000 μg/ml. There were some variations among the sublines, but five *PRPS1*-mutated sublines and parental cells showed almost similar sensitivities.

Discussion

In the present study, we applied the CRISPR/Cas9 system to induce the relapse-specific mutations of the *NT5C2* and *PRPS1* genes. Considering the off-target score of the target site, we selected the R39Q mutation of the *NT5C2* gene and the S103N mutation of the *PRPS1* gene as candidates. Although most of the 6-MP–resistant sublines were mixed populations of diverse mutations at the target sites, we successfully obtained the sublines that homozygously acquired the intended mutations with the designed silent mutations as a result of HR. Recently, Yang et al. (2021) reported the possibility that long-term treatment of 6-MP induces C>T type mutation of the *TP53* gene in ALL cells. However, our ddPCR analyses in the parental cells treated with 6-MP for drug selection (500 nM for 2 weeks) demonstrated that expansion of the minor clones with the *NT5C2*-R39Q or *PRPS1*-S103N mutations was unlikely. Interestingly, all of the other sublines acquired diverse in-frame mutations at the target sites as a result of indels due to NHEJ. These observations indicated the crucial involvement of target residues of NT5C2 and PRPS1 in the negative regulation of their catalytic activities.

R39Q mutation of the *NT5C2* gene induces the substitution of the basic amino acid (Arg) to polar amino acid (Glu). As a result, the switch-off mechanism was disrupted by static alteration of the positively charged intermonomeric pocket region, which is involved in the regulation from closed inactive configuration to open active configuration (Dieck et al., 2018). In the other *NT5C2* mutations observed in the present study, adjacent Leu^{41}-Ala^{42} residues were substituted to Thr-Thr or Leu-Gly-Pro due to small in-frame indels at the target site. Leu^{41} and Ala^{42} residues are nonpolar amino acids and located in intermediate portions between β-strand (36–39 residues) and helix (43–45 residues) structures. Despite these substituted amino acids also being nonpolar amino acids, except for Thr (polar amino acid), these substitutions may structurally affect the adjacent pocket region and, subsequently, disrupt the switch-off mechanism. Further structural analysis of these *NT5C2* mutations may provide a deeper understanding of the significance of Leu^{41} and Ala^{42} residues in the regulation of NT5C2 catalytic activity.

In the *PRPS1* mutations observed in our sublines, small in-frame indels induced by NHEJ were observed at the target site in addition to the S103N mutation induced by HR. Previous crystal structure analysis of human PRPS1 revealed that the flexible loop of Lys^{100}–Arg^{104} residues forms the allosteric site in which GDP or ADP binding negatively regulates catalytic activity of PRPS1 (Li et al., 2007). In the relapsed ALL cases, S103T, S103I, and S103N were identified (Li et al., 2015). Thus, although polar uncharged Ser^{103} is substituted to the same polar uncharged Asn, Thr, or Ile, structural changes induced by these mutations may affect the binding property of nucleotide inhibitors at the allosteric site (Li et al., 2015). In the present study, S103L mutation was also observed in the established sublines. Considering the substitution of polar uncharged Ser^{103} to nonpolar Leu, S103L may heavily affect the structure of the allosteric site. In the other mutations observed in the present study, nonpolar amino acids (Gly, Ala, Leu, or Pro) were inserted just in front of the Ser^{103} residue. These mutations may also disrupt the negative regulation of PRPS1 catalytic activity due to structural changes in the allosteric site.

For the induction of *PRPS1*-S103N mutation by the CRISPR/Cas9 system, codon 103 locates at the 5′ end of exon 3. Of note, we confirmed that one of the 6-MP–resistant sublines harbored indels in the 3′ end of intron 2 but not in the coding exon 3. In this mutation, the wild-type sequence of "atttag" at the 3′ end of intron 2 was substituted to "ccaaca," resulting in the disruption of the splicing acceptor consensus sequence (NYAG). Indeed, we confirmed the RT-PCR product corresponding to this mutation, in which exon 2 was directly ligated to exon 4. Thus, PRPS1 protein derived from this transcript is supposed to lack 33 amino acids corresponding to the residues 103–135 encoded by exon 3 but still retain catalytic domain encoded by exons 5 and 6. Although precise structural significances of this mutation remain to be elucidated, this aberrant splicing variant may heavily disrupt the structure of the allosteric site.

As one of the thiopurine-resistant mechanisms, we evaluated the ABCC4 expression level and confirmed almost similar expression levels between the parental cells and the 6-MP–resistant sublines. Moreover, although upregulation of NT5C2 or PRPS1 is potentially associated with thiopurine resistance, we confirmed that NT5C2 and PRPS1 protein expression levels were not upregulated in the *NT5C2* and *PRPS1*-mutated sublines in comparison with those in the parental cells, respectively. Of note, gene and protein expression levels of PRPS1 in the *PRPS1*-mutated sublines were rather downregulated, suggesting that mutations adjacent to codon 103 might somehow affect the stability of *PRPS1* transcripts. Finally, we confirmed that sensitivities to daunorubicin, vincristine, and dasatinib were almost identical between the parental cells and the *NT5C2* and *PRPS1*-mutated sublines. These observations strongly suggested that *NT5C2* and *PRPS1*-mutated sublines acquired specific resistance to thiopurine due to the acquisition of *NT5C2* and *PRPS1* mutations.

In the present study, we confirmed that the sublines with *NT5C2*-R39Q and *PRPS1*-S103N mutations were resistant to 6-MP at the pharmacological concentration in 7-day exposure assay, whereas the parental cells were highly sensitive. Although we have not tested the in vivo 6-MP–resistant phenotypes of our *NT5C2*-R39Q and *PRPS1*-S103N sublines, a previously established knock-in mouse model of the tamoxifen-inducible expression of *Nt5c2*-R367Q mutation revealed the 6-MP–resistant phenotype in vivo (Tzoneva et al., 2018). Consistently, we confirmed that intracellular TIMP levels in the *NT5C2*-R39Q and *PRPS1*-S103N sublines were ly lower than that in the parental cells after sequential 6-hour exposure to 6-MP at the concentrations that mimic pharmacokinetics during maintenance therapy (Balis et al., 1998). Although the sublines with *NT5C2*-R39Q and *PRPS1*-S103N mutations were remarkably more resistant to 6-TG than the parental cells, the IC_{50} values of 6-TG in the sublines were below the serum C_{max} level during maintenance therapy (Lennard et al., 1993). In previous clinical randomized studies with 6-MP versus 6-TG

for maintenance therapy, it has been demonstrated that 6-TG caused excessive adverse events without improving therapeutic outcomes in comparison with 6-MP (Harms et al., 2003; Vora et al., 2006; Stork et al., 2010). However, our observations suggested the possibility that the standard dose of 6-TG might be effective for relapsed ALL patients with *NT5C2* and *PRPS1* mutations.

Consistent with previous reports, we confirmed that the sublines with *NT5C2* mutations were remarkably more sensitive to MPA (Stet et al., 1993; Tzoneva et al., 2018). These observations suggested that IMPDH inhibitors might be useful for relapsed ALL patients with *NT5C2* mutation. In contrast to *NT5C2* mutations, we could not confirm the utility of 5-FU in the *PRPS1*-mutated sublines. The previous report indicated that ALL cell line (Reh) transfected with S103T mutant *PRPS1* cDNA was remarkably more sensitive to 5-FU than that transfected with wild-type *PRPS1* cDNA (Wang et al., 2018). The IC_{50} value of 5-FU in the parental Reh was reported to be 4.5 μg/ml. In contrast to Reh, the IC_{50} value of 5-FU in the parental KOPN55bi was over 2000 μg/ml. Thus, KOPN55bi might not be suitable to test the significance of *PRPS1* mutation in 5-FU sensitivity because of its intrinsic 5-FU resistance. Another difference between the previous report and the present study is the possible involvement of transcriptional and post-transcriptional regulation. In the previous study, in addition to the intrinsic wild-type *PRPS1* expression, either wild-type or mutated *PRPS1* cDNA was transduced with a lentiviral vector (Wang et al., 2018). In the present study, the significance of the *PRPS1* mutation was evaluated in the intrinsic gene. Moreover, gene and protein expression levels of PRPS1 were rather downregulated in our mutated sublines. Thus, these differences in the PRPS1 expression levels might be somehow associated with differences in 5-FU sensitivity.

In summary, we successfully introduced hotspot relapse-specific mutations of the *NT5C2* and *PRPS1* genes into a human lymphoid leukemia cell line as a result of HR using the CRISPR/Cas9 system. Moreover, we confirmed diverse in-frame mutations at the target sites as a result of NHEJ. These cellular systems enable the evaluation of pharmacological and structure-biologic significances of the hotspot mutations under the control of the intrinsic gene regulation. Our model will be a novel, valuable tool for developing new therapeutic approaches to overcome thiopurine resistance in relapsed ALL.

Authorship Contributions

Participated in research design: Nguyen, Tamai, Inukai.

Conducted experiments: Nguyen, Tanaka, Sanada, Hosaka, Tamai, Kagami, Komatsu.

Contributed new reagents or analytic tools: Tanaka, Sanada, Hosaka.

Performed data analysis: Nguyen, Kagami, Komatsu, Harama, Kasai, Somazu, Watanabe, Akahane, Goi.

Wrote or contributed to the writing of the manuscript: Nguyen, Inukai.

References

Balis FM, Holcenberg JS, Poplack DG, Ge J, Sather HN, Murphy RF, Ames MM, Waskerwitz MJ, Tubergen DG, Zimm S, et al. (1998) Pharmacokinetics and pharmacodynamics of oral methotrexate and mercaptopurine in children with lower risk acute lymphoblastic leukemia: a joint children's cancer group and pediatric oncology branch study. *Blood* **92**:3569–3577.

Black KL, Naqvi AS, Asnani M, Hayer KE, Yang SY, Gillespie E, Bagashev A, Pillai V, Tasian SK, Gazzara MR, et al. (2018) Aberrant splicing in B-cell acute lymphoblastic leukemia. *Nucleic Acids Res* **46**:11357–11369.

Cortes JE and Kantarjian HM (1995) Acute lymphoblastic leukemia. A comprehensive review with emphasis on biology and therapy. *Cancer* **76**:2393–2417.

Dieck CL and Ferrando A (2019) Genetics and mechanisms of NT5C2-driven chemotherapy resistance in relapsed ALL. *Blood* **133**:2263–2268.

Dieck CL, Tzoneva G, Forouhar F, Carpenter Z, Ambesi-Impiombato A, Sánchez-Martín M, Kirschner-Schwabe R, Lew S, Seetharaman J, Tong L, et al. (2018) Structure and Mechanisms of NT5C2 Mutations Driving Thiopurine Resistance in Relapsed Lymphoblastic Leukemia. *Cancer Cell* **34**:136–147.e6.

Evensen NA, Madhusoodhan PP, Meyer J, Saliba J, Chowdhury A, Araten DJ, Nersting J, Bhatla T, Vincent TL, Teachey D, et al. (2018) MSH6 haploinsufficiency at relapse contributes to the development of thiopurine resistance in pediatric B-lymphoblastic leukemia. *Haematologica* **103**:830–839.

Ferreira PCL, Thiesen FV, Pereira AG, Zimmer AR, and Fröehlich PE (2020) A short overview on mycophenolic acid pharmacology and pharmacokinetics. *Clin Transplant* **34**:e13997.

Harms DO, Göbel U, Spaar HJ, Graubner UB, Jorch N, Gutjahr P, and Janka-Schaub GE; COALL Study Group (2003) Thioguanine offers no advantage over mercaptopurine in maintenance treatment of childhood ALL: results of the randomized trial COALL-92. *Blood* **102**:2736–2740.

Hoell JI, Ginzel S, Kuhlen M, Kloetgen A, Gombert M, Fischer U, Hein D, Demir S, Stanulla M, Schrappe M, et al. (2019) Pediatric ALL relapses after allo-SCT show high individuality, clonal dynamics, selective pressure, and druggable targets. *Blood Adv* **3**:3143–3156.

Hunger SP and Mullighan CG (2015) Acute Lymphoblastic Leukemia in Children. *N Engl J Med* **373**:1541–1552.

Inaba H and Mullighan CG (2020) Pediatric acute lymphoblastic leukemia. *Haematologica* **105**:2524–2539.

Karran P and Attard N (2008) Thiopurines in current medical practice: molecular mechanisms and contributions to therapy-related cancer. *Nat Rev Cancer* **8**:24–36.

Ko RH, Ji L, Barnette P, Bostrom B, Hutchinson R, Raetz E, Seibel NL, Twist CJ, Eckroth E, Sposto R, et al. (2010) Outcome of patients treated for relapsed or refractory acute lymphoblastic leukemia: a Therapeutic Advances in Childhood Leukemia Consortium study. *J Clin Oncol* **28**:648–654.

Kolenova A, Maloney KW, and Hunger SP (2016) Philadelphia Chromosome-positive Acute Lymphoblastic Leukemia or Chronic Myeloid Leukemia in Lymphoid Blast Crisis. *J Pediatr Hematol Oncol* **38**:e193–e195.

Lennard L, Davies HA, and Lilleyman JS (1993) Is 6-thioguanine more appropriate than 6-mercaptopurine for children with acute lymphoblastic leukaemia? *Br J Cancer* **68**:186–190.

Li B, Brady SW, Ma X, Shen S, Zhang Y, Li Y, Szlachta K, Dong L, Liu Y, Yang F, et al. (2020) Therapy-induced mutations drive the genomic landscape of relapsed acute lymphoblastic leukemia. *Blood* **135**:41–55.

Li B, Li H, Bai Y, Kirschner-Schwabe R, Yang JJ, Chen Y, Lu G, Tzoneva G, Ma X, Wu T, et al. (2015) Negative feedback-defective PRPS1 mutants drive thiopurine resistance in relapsed childhood ALL. *Nat Med* **21**:563–571.

Li S, Lu Y, Peng B, and Ding J (2007) Crystal structure of human phosphoribosylpyrophosphate synthetase 1 reveals a novel allosteric site. *Biochem J* **401**:39–47.

Malard F and Mohty M (2020) Acute lymphoblastic leukaemia. *Lancet* **395**:1146–1162.

Maruyama T, Dougan SK, Truttmann MC, Bilate AM, Ingram JR, and Ploegh HL (2015) Increasing the efficiency of precise genome editing with CRISPR-Cas9 by inhibition of nonhomologous end joining. *Nat Biotechnol* **33**:538–542.

Mayr C and Bartel DP (2009) Widespread shortening of 3'UTRs by alternative cleavage and polyadenylation activates oncogenes in cancer cells. *Cell* **138**:673–684.

Meyer JA, Wang J, Hogan LE, Yang JJ, Dandekar S, Patel JP, Tang Z, Zumbo P, Li S, Zavadil J, et al. (2013) Relapse-specific mutations in NT5C2 in childhood acute lymphoblastic leukemia. *Nat Genet* **45**:290–294.

Moriyama T, Nishii R, Perez-Andreu V, Yang W, Klussmann FA, Zhao X, Lin T-N, Hoshitsuki K, Nersting J, Kihira K, et al. (2016) NUDT15 polymorphisms alter thiopurine metabolism and hematopoietic toxicity. *Nat Genet* **48**:367–373.

Naffouje R, Grover P, Yu H, Sendilnathan A, Wolfe K, Majd N, Smith EP, Takeuchi K, Senda T, Kofuji S, et al. (2019) Anti-Tumor Potential of IMP Dehydrogenase Inhibitors: A Century-Long Story. *Cancers (Basel)* **11**:1346.

Patel SA, Bledsoe JR, Higgins AW, Hutchinson L, and Gerber JM (2021) Rapid and Deep Remission Induced by Blinatumomab for CD19-Positive Chronic Myeloid Leukemia in Lymphoid Blast Phase. *JCO Precision Oncology* **5**:1141–1146.

Peng X-X, Shi Z, Damaraju VL, Huang X-C, Kruh GD, Wu H-C, Zhou Y, Tiwari A, Fu L, Cass CE, et al. (2008) Up-regulation of MRP4 and down-regulation of influx transporters in human leukemic cells with acquired resistance to 6-mercaptopurine. *Leuk Res* **32**:799–809.

Sandberg R, Neilson JR, Sarma A, Sharp PA, and Burge CB (2008) Proliferating cells express mRNAs with shortened 3′ untranslated regions and fewer microRNA target sites. *Science* **320**:1643–1647.

Shaul O (2017) How introns enhance gene expression. *Int J Biochem Cell Biol* **91**:145–155.

Somazu S, Tanaka Y, Tamai M, Watanabe A, Kagami K, Abe M, Harama D, Shinohara T, Akahane K, Goi K, et al. (2021) NUDT15 polymorphism and NT5C2 and PRPS1 mutations influence thiopurine sensitivity in acute lymphoblastic leukaemia cells. *J Cell Mol Med* **25**:10521–10533.

Song J, Yang D, Xu J, Zhu T, Chen YE, and Zhang J (2016) RS-1 enhances CRISPR/Cas9- and TALEN-mediated knock-in efficiency. *Nat Commun* **7**:10548.

Stet EH, De Abreu RA, Janssen YPG, Bökkerink JPM, and Trijbels FJM (1993) A biochemical basis for synergism of 6-mercaptopurine and mycophenolic acid in Molt F4, a human malignant T-lymphoblastic cell line. *Biochim Biophys Acta* **1180**:277–282.

Stork LC, Matloub Y, Broxson E, La M, Yanofsky R, Sather H, Hutchinson R, Heerema NA, Sorrell AD, Masterson M, et al. (2010) Oral 6-mercaptopurine versus oral 6-thioguanine and veno-occlusive disease in children with standard-risk acute lymphoblastic leukemia: report of the Children's Oncology Group CCG-1952 clinical trial. *Blood* **115**:2740–2748.

Tamai M, Inukai T, Kojika S, Abe M, Kagami K, Harama D, Shinohara T, Watanabe A, Oshiro H, Akahane K, et al. (2018) T315I mutation of BCR-ABL1 into human Philadelphia chromosome-positive leukemia cell lines by homologous recombination using the CRISPR/Cas9 system. *Sci Rep* **8**:9966.

Tatsumi G, Kawahara M, Imai T, Nishishita-Asai A, Nishida A, Inatomi O, Yokoyama A, Kakuta Y, Kito K, and Andoh A (2020) Thiopurine-mediated impairment of hematopoietic stem and leukemia cells in Nudt15^{R138C} knock-in mice. *Leukemia* **34**:882–894.

Tzoneva G, Dieck CL, Oshima K, Ambesi-Impiombato A, Sánchez-Martín M, Madubata CJ, Khiabanian H, Yu J, Waanders E, Iacobucci I, et al. (2018) Clonal evolution mechanisms in NT5C2 mutant-relapsed acute lymphoblastic leukaemia. *Nature* **553**:511–514.

Tzoneva G, Perez-Garcia A, Carpenter Z, Khiabanian H, Tosello V, Allegretta M, Paietta E, Racevskis J, Rowe JM, Tallman MS, et al. (2013) Activating mutations in the NT5C2 nucleotidase gene drive chemotherapy resistance in relapsed ALL. *Nat Med* **19**:368–371.

Uno K, Inukai T, Kayagaki N, Goi K, Sato H, Nemoto A, Takahashi K, Kagami K, Yamaguchi N, Yagita H, et al. (2003) TNF-related apoptosis-inducing ligand (TRAIL) frequently induces apoptosis in Philadelphia chromosome-positive leukemia cells. *Blood* **101**:3658–3667.

Vora A, Mitchell CD, Lennard L, Eden TO, Kinsey SE, Lilleyman J, and Richards SM; Medical Research Council; National Cancer Research Network Childhood Leukaemia Working Party (2006) Toxicity and efficacy of 6-thioguanine versus 6-mercaptopurine in childhood lymphoblastic leukaemia: a randomised trial. *Lancet* **368**:1339–1348.

Wahlund M, Nilsson A, Kahlin AZ, Broliden K, Myrberg IH, Appell ML, and Berggren A (2020) The Role of TPMT, ITPA, and NUDT15 Variants during Mercaptopurine Treatment of Swedish Pediatric Patients with Acute Lymphoblastic Leukemia. *J Pediatr* **216**:150–157.e1.

Wang D, Chen Y, Fang H, Zheng L, Li Y, Yang F, Xu Y, Du L, Zhou BS, and Li H (2018) Increase of PRPP enhances chemosensitivity of PRPS1 mutant acute lymphoblastic leukemia cells to 5-Fluorouracil. *J Cell Mol Med* **22**:6202–6212.

Wu C and Li W (2018) Genomics and pharmacogenomics of pediatric acute lymphoblastic leukemia. *Crit Rev Oncol Hematol* **126**:100–111.

Yadav B, Wennerberg K, Aittokallio T, and Tang J (2015) Searching for Drug Synergy in Complex Dose-Response Landscapes Using an Interaction Potency Model. *Comput Struct Biotechnol J* **13**:504–513.

Yang F, Fang H, Wang D, Chen Y, Zhai Y, Zhou S, and Li H (2018) HPRT1 activity loss is associated with resistance to thiopurine in ALL. *Oncotarget* **9**:2268–2278.

Yang F, Brady SW, Tang C, Sun H, Du L, Barz MJ, Ma X, Chen Y, Fang H, Li X, et al. (2021) Chemotherapy and mismatch repair deficiency cooperate to fuel TP53 mutagenesis and ALL relapse. *Nat Can* **2**:819–834.

Zheng S, Wang W, Aldahdooh J, Malyutina A, Shadbahr T, Tanoli Z, Pessia A, and Tang J (2022) SynergyFinder Plus: Toward Better Interpretation and Annotation of Drug Combination Screening Datasets. *Genomics Proteomics Bioinformatics* **20**: 587–596.

Address correspondence to: Dr. Takeshi Inukai, Department of Pediatrics, School of Medicine, University of Yamanashi, 1110 Shimokato, Chuo, Yamanashi 409-3898, Japan. E-mail: tinukai@yamanashi.ac.jp

Supplemental Data

Molecular Pharmacology

CRISPR/Cas9-mediated induction of relapse-specific *NT5C2* and *PRPS1* mutations confers thiopurine resistance as a relapsed lymphoid leukemia model

Thao Thu Thi Nguyen[1], Yoichi Tanaka[2], Masashi Sanada[3], Masumi Hosaka[3], Minori Tamai[1], Keiko Kagami[1], Chiaki Komatsu[1], Shinpei Somazu[1], Daisuke Harama[1], Shin Kasai[1], Atsushi Watanabe[1], Koushi Akahane[1], Kumiko Goi[1], Takeshi Inukai[1]

Supplemental Figures

Supplemental Fig. S1 Sanger sequencing of the coding regions of the *NT5C2* gene (A) and *PRPS1* gene (B) in parental cells and the *NT5C2*-R39Q or *PRPS1*-S103N mutated subline. At the top of each panel, the protein-coding regions of each gene are indicated in green, and untranslated regions are indicated in grey. The black arrowheads indicate the binding sites of primers used for sanger sequencing. Targeted codon 39 of the *NT5C2* gene is highlighted in yellow, and targeted codon 103 of the *PRPS1* gene is highlighted in blue. The PAM sites are underlined. Red characters indicate nucleotide substitutions in the mutated sublines.

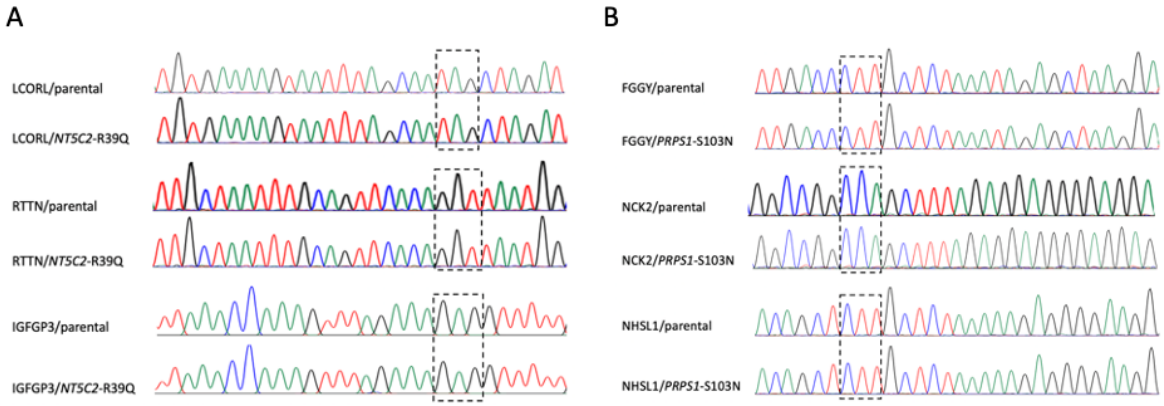

Supplemental Fig. S2 Off-target edit analysis. **(A)** Direct sequencing of the genomic PCR products from *NT5C2*-R39Q subline and parental cells at three possible off-target sites located in the *FGGY, NCK2,* and *NHSL1* genes. **(B)** Direct sequencing of the genomic PCR products from *PRPS1*-S103N subline and parental cells at three possible off-target sites located in the *FGGY, NCK2,* and *NHSL1* genes. The dash boxes indicate the PAM sites of each target.

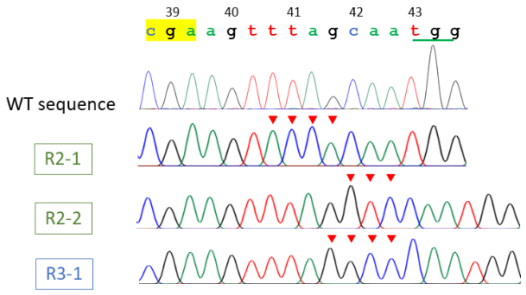

Supplemental Fig. S3 Sanger sequencing of the genomic PCR products after TA cloning in *NT5C2*-mutated sublines. Targeted codon 39 is highlighted in yellow, and the PAM site is underlined. Red arrowheads indicate nucleotide substitutions.

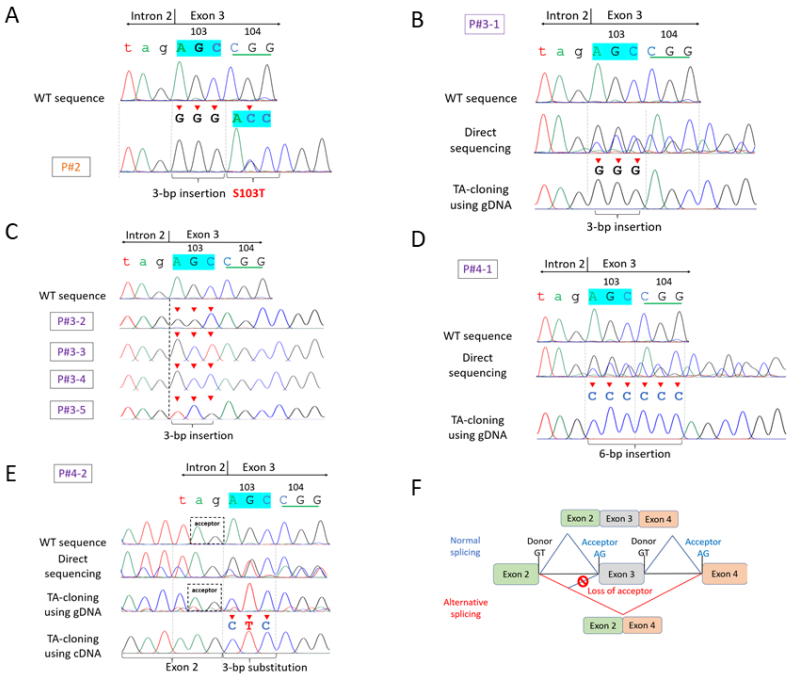

Supplemental Fig. S4 Inframe indels and exon skipping due to non-homologous end-joining at the target site in *PRPS1*-mutated sublines. **(A)** Sanger sequencing of the genomic PCR products in subline P#2. Intron 2-exon 3 boundary was indicated at the top of the panel. Red arrowheads indicate nucleotide substitutions. **(B-E)** Sanger sequencing of the genomic PCR products after TA cloning in subline P#3 and P#4. Red arrowheads indicate nucleotide substitutions. Dash line indicates intron 2-exon 3 boundary. Dash boxes indicate splice site acceptor. **(F)** Illustration of exon 3 skipping in subline P#5. The splicing acceptor consensus sequence at the 3' end of intron 2 was completely disrupted as a result of an indel, which resulted in the skipping of exon 3.

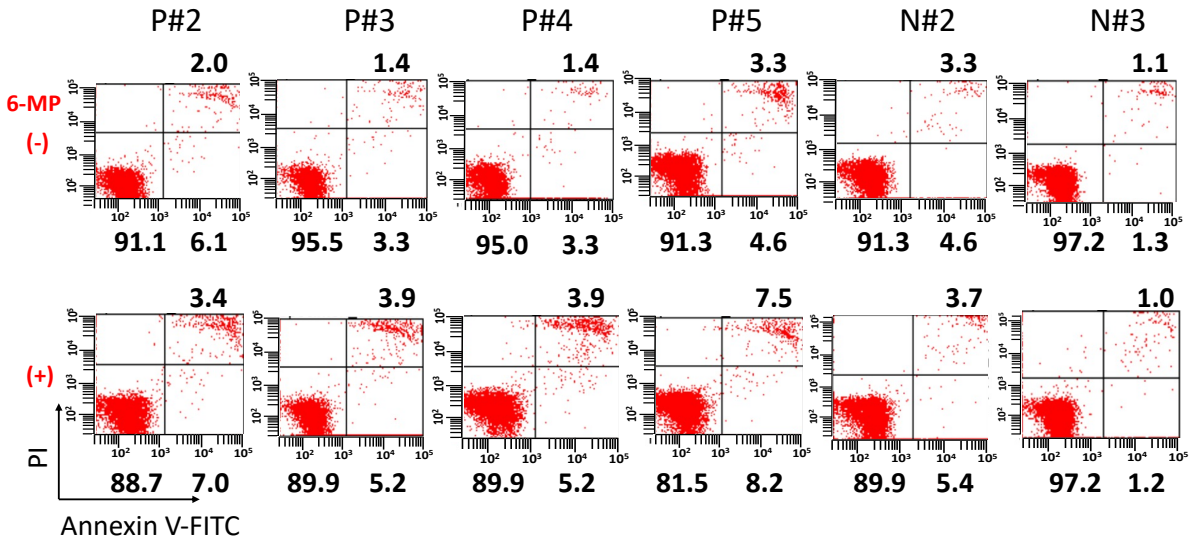

Supplemental Fig. S5 Reduced apoptosis after 7-day exposure to 200 nM of 6-MP in *NT5C2*-mutated sublines N#2-3 and *PRPS1*-mutated sublines P#3-5. Flow cytometric analysis of annexin V-binding and PI staining is indicated. The percentages of living cells (lower-left), early apoptotic cells (lower-right), and late apoptotic cells (upper-light) are indicated in the corner of each panel.

Supplemental Tables

Suplemental Table S1. Primer for PCR and RT-PCR analyses

Primers	**Target**	**Sequence (5'- 3')**
NT5C2-39-F	codon 39	CAAACAGCATGTCGTGTTATACAT
NT5C2-39-R	codon 39	TCATGAGCCACATCTCAAGG
PRPS1-RT-F	for RT-PCR	CCGTGATCGCTTAGTGGAGT
PRPS1-RT-R	for RT-PCR	ACCAGCATCAGGTGAGACAA
PRPS1-103-F	codon 103	TTCTGGGTACCATAGTGCCTTT
PRPS1-103-R	codon 103	TTTGGCTTCTCTGCAGTCTTC
NT5C2-seq-F	*NT5C2* coding region	CTCTGCTGCCCAGGCTGGAGTA
NT5C2-seq-R	*NT5C2* coding region	GCTTGGGGCCATGTGGGAAGTC
NT5C2-seq-F1	*NT5C2* coding region	AGACCTACCTGTTGGCCTGCCT
NT5C2-seq-R1	*NT5C2* coding region	ACATGGGCAGCCCTGAAGAGGT
NT5C2-seq-F2	*NT5C2* coding region	GACTTCCCACATGGCCCCAAGC
NT5C2-seq-R2	*NT5C2* coding region	TCCCTCCCCCGAGTAGAACCCT
PRPS1-seq-F	*PRPS1* coding region	GGTCTCTGCAGCAGCCGTGATC
PRPS1-seq-R	*PRPS1* coding region	ACTGGAGCAAGCCGGGTCTTCT
OFT-*IGFBP3*-F	off-target site	GGCCCTTCCCCAGGCTTACAGA
OFT-*IGFBP3*-R	off-target site	AGTCTGGGTGCTGTGCTCGAGT
OFT-*RTTN*-F	off-target site	TGTTTTGTCCGCTTTCCCAGGGA
OFT-*RTTN*-R	off-target site	TCCAGTGGCATCTGGGAAGCCA
OFT-*LCORL*-F	off-target site	TGCCAGCCCCTTCAGAAAGCAC
OFT-*LCORL*-R	off-target site	CCCTCTGCTGCAAGTCACCCCT
OFT-*FGGY*-F	off-target site	ACGCCCCCAAAGCTGACAAAGG
OFT-*FGGY*-R	off-target site	CCTCTGGGGCTTGACCTGGTGA
OFT-*NHSL1*-F	off-target site	AGAAGTGGTCTTATGGGCTCAA
OFT-*NHSL1*-R	off-target site	AGTCACTCAGTTGTGTGTAGCAT
OFT-*NCK2*-F	off-target site	AAAGGCGCCCATCTTCACCAGC
OFT-*NCK2*-R	off-target site	TGCACAGTCCGGGAGCCATGTA

Supplemental Table S2: Incidences of *NT5C2*-R39Q and *PRPS1*-S103N mutations after exposure to 6-MP

Sample	Target	Incidence (%)	Target	Incidence (%)
Parental cells/ 100 nM - 1 week	*NT5C2*-R39Q	0	*PRPS1*-S103N	0.03
Parental cells/ 100 nM - 2 week	*NT5C2*-R39Q	0.011	*PRPS1*-S103N	0.014
Parental cells/ 100 nM - 4 week	*NT5C2*-R39Q	0.004	*PRPS1*-S103N	0.011
Parental cells/ 200 nM - 1 week	*NT5C2*-R39Q	0.007	*PRPS1*-S103N	0.037
Parental cells/ 200 nM - 2 week	*NT5C2*-R39Q	0.011	*PRPS1*-S103N	0.005
Parental cells/ 200 nM - 4 week	*NT5C2*-R39Q	0.004	*PRPS1*-S103N	0.007
Parental cells/ 500 nM - 1 week	*NT5C2*-R39Q	0.009	*PRPS1*-S103N	0.021
Parental cells/ 500 nM - 2 week	*NT5C2*-R39Q	0.011	*PRPS1*-S103N	0.005
Buffy DNA (negative control)	*NT5C2*-R39Q	0.007	*PRPS1*-S103N	0

Supplemental Table S3. Cell viability (%) under combined treatment of MPA with 6-MP

MPA (nM) / 6-MP (nM)	(-)	78.1	156.2	312.5	625	1250	2500
(-)	100.0	99.6	97.5	93.6	100.3	34.2	2.9
12.4	97.9	98.2	97.2	93.5	105.0	31.1	1.4
37.0	99.1	105.2	102.5	95.1	104.1	33.5	1.8
111.1	102.2	102.7	101.8	96.7	103.2	32.1	1.8
333.3	101.0	102.0	101.8	94.4	102.3	30.5	1.4
1000.0	99.5	94.0	96.4	89.6	96.1	28.0	1.8
3000.0	86.9	74.2	51.1	39.6	50.3	27.1	1.9